Thermocapillary flow of a thin liquid film in a confined two-layer system under a hydrophobic plate

Valeri Frumkin and Alexander Oron
Department of Mechanical Engineering, Technion–Israel Institute of Technology, Haifa 32000, Israel
(Received 13 June 2017; published 26 October 2017)

We investigate flow in a thin liquid film over a heated solid surface in a bilayer two-dimensional gas-liquid system bounded on the gas side by an isothermal hydrophobic plate. The flow is driven by the Marangoni instability induced, in one case, by a thermal wave propagating along a flat solid substrate on the liquid side and in the other case by a left-right asymmetric topography of the thick solid substrate adjacent to the liquid phase uniformly heated at its outer surface. Using a long-wave approximation, we derive a nonlinear evolution equation governing the spatiotemporal dynamics of the liquid-gas interface and derive a closed-form expression indicating a nonzero value for a liquid flow rate in a steady state of the system, if attained. Numerical investigation is carried out to study the nonlinear dynamics of the gas-liquid interface and the resulting flow for various values of the system parameters. A linear stability analysis of the two-dimensional steady states of the system with a two-dimensional corrugated substrate on the liquid side is carried out with respect to three-dimensional out-of-plane disturbances. We demonstrate that the presence of a hydrophobic substrate enables a continuous flow for narrow systems associated with low values of the ratio between the mean thickness of the gas layer to that of the liquid, which would be impossible in its absence. This represents an extension of the conceptual methods discussed in our previous studies for the control and amplification of the average flow rate through the system for narrow systems, thus allowing for efficient thermocapillary transport in extremely small microfluidic devices.

DOI: 10.1103/PhysRevFluids.2.104002

I. INTRODUCTION

An ability to transport liquids and particles through microchannels is of central importance in the field of microfluidics and laboratory-on-a-chip technologies [1,2]. Flows inside a microchannel can be driven by body forces, e.g., gravity, electric or magnetic, or by surface-tension gradients when fluid-fluid interfaces are present. The latter mechanism leads to the emergence of the Marangoni effect [3] caused by temperature variations [4], differences in chemical composition [5], wettability [6], or electrical potential gradients [7,8]. Following Pearson's seminal paper [9], which attributed the formation of Bénard cells [10] to the presence of surface-tension gradients caused by heat transfer, much attention has been devoted to the investigation of this effect, referred to in the literature [11,12] as the thermocapillary or Marangoni effect, and its possible applications for controlling the dynamics of fluid-fluid interfaces including recent applications of thermocapillarity in microfluidics [13].

Due to the fact that strong thermal motion of fluid particles at the free surface of a liquid film have a diminishing effect on the net attraction forces experienced by each particle, a local increase of the temperature on the free surface normally leads to a local decrease in the surface tension. As a result, an uneven temperature distribution at the surface of a liquid film causes colder regions with higher surface tension to pull liquid from the warmer regions, leading via fluid viscosity to convective motion driven by interfacial flow. If the temperature difference across the system is sufficiently strong, long-wave instability [14] sets in, leading to the deformation of the free surface and finally to film rupture [15,16]. The dimensionless parameter governing the dynamics of this instability is the Marangoni number M, which represents a dimensionless version of the temperature difference across the system expressed as the ratio between the thermocapillary and dissipative forces, the latter due to fluid viscosity and thermal diffusivity.

Using long-wave expansions, a nonlinear spatiotemporal evolution equation of the gas-liquid interface was derived [11,16–18], accounting for the effects of gravity, capillarity, and thermocapillarity. All said, the above is related to systems consisting of a liquid layer supported from below by a solid heated wall and bounded from above by an unbounded ambient gas phase. Two-layer systems subjected to the action of the Marangoni effect composed of superimposed liquid and gas layers enclosed between two solid substrates were investigated by Golovin *et al.* [19] and VanHook *et al.* [20].

Kumar and co-workers [21,22] considered various problems related to two fluid-layer confined systems. Steady two-layer thin film flows in topographically patterned channels with isolated or periodic corrugation were studied [21]. It was demonstrated that large pressure gradients arising due to the presence of the bounded geometry can fully suppress interfacial features that are present in a single-layer flow over topographically patterned surfaces. Kalpathy *et al.* [22] showed that shear may delay or even prevent rupture in two-layer systems subjected to van der Waals interactions. This result is qualitatively similar to that obtained by Davis *et al.* [23] for a single-layer system.

Breaking the left-to-right symmetry of a horizontal setting, by an imposed lateral temperature gradients [4,24], traveling thermal waves [25,26], or in the presence of asymmetric topography of the underlying substrate [27–29], may induce nonzero net flow along the system, thus providing efficiency to the thermocapillary transport of liquids and droplets in microfluidic devices. In this paper we deal with a problem arising in a typical two-layer system consisting of a horizontal thin liquid film underlying a gas layer, sandwiched between a heat-conducting substrate of either flat or a general periodic topography from below and a flat isothermal upper wall from above. If the ratio δ of the thickness of the gas layer to that of the liquid is sufficiently large, for values of M above a certain critical threshold, the liquid film will rupture at the underlying substrate [20,29]. If, however, δ is small, as the liquid-gas interface deforms, it will rupture at the upper wall and become pinned there [20] as it comes into contact with the wall. Since the main flow-driving mechanism in our system is liquid flow originating at the gas-liquid interface, such pinning will locally terminate the action of the Marangoni effect and halt flow through the system. This feature leads to the existence of a lower bound for the thickness of the gas layer depending on the rest of the system parameters, which causes separation between the liquid film and the upper wall, for which the emerging through flow remains continuous.

In order to enable the flow to be continuous with no rupture for even smaller systems, we introduce an effective slippage at the upper wall into our configuration, by taking the upper surface to be hydrophobic. This interaction between molecules of the liquid and the hydrophobic substrate is modeled by a repulsive disjoining pressure potential. Several works [30–32] give a comprehensive review of theoretical and experimental results in the study of slippage phenomena at the fluid-solid interface.

The purpose of this paper is to extend the results of our previous studies [26,29] by adding hydrophobicity of the wall on the gas side of the system and to explore the properties of the augmented setting. The structure of the paper is as follows. Section II presents the problem statement and the evolution equation governing the nonlinear dynamics of the system. Section III is dedicated to the presentation of results of the investigation and their discussion. In Sec. IV we present an extension of the study carried out in Sec. III to the case of a three-dimensional dynamics of the system. A summary and closing remarks are given in Sec. V.

II. PROBLEM DEFINITION AND EVOLUTION EQUATION

We consider a horizontal two-dimensional system consisting of a liquid film resting on an either thin flat or thick heat-conducting solid substrate of a general periodic geometry and flat from underneath, and a gas layer overlying the liquid film and bounded from above by a flat horizontal hydrophobic plate. Due to the small size of the system under consideration, gravity is excluded from the analysis. By saying that the lower substrate may be thick we mean that its

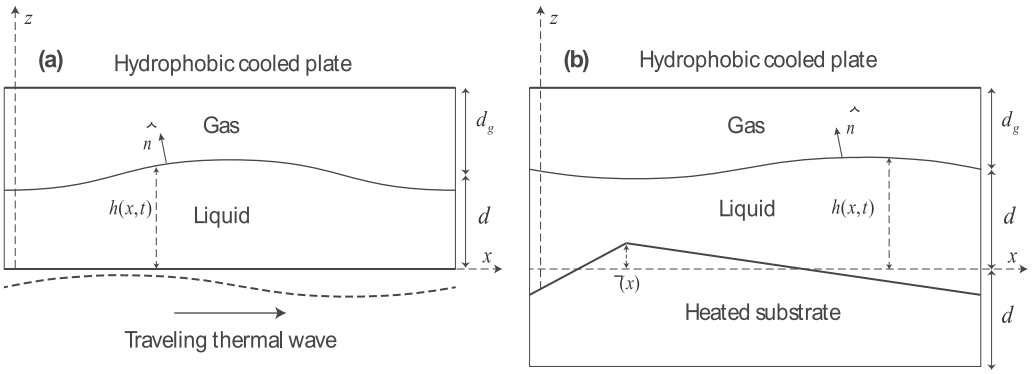

FIG. 1. Sketch of the systems in the two cases considered here. (a) The underlying substrate is flat with an imposed traveling thermal wave. (b) The underlying substrate is asymmetrically and periodically corrugated and uniformly heated from below.

thickness is not infinitesimal but finite. The outer side of the substrate adjacent to the liquid film is heated to the temperature $\theta_b(x,t) = \bar{\theta}_b(1 + A\tilde{f}(x,t))$, with $A \geqslant 0$ and $\tilde{f}(x,t)$ representing the shape of the thermal wave slowly varying in time t and space x with the spatial average $\bar{\theta}_b$, whereas the upper plate of an infinitesimal thickness is maintained at the constant temperature θ_t so that $\Delta\theta \equiv \bar{\theta}_b - \theta_t > 0$. Note that, in the case of $A = 0$, the imposed temperature on the lower substrate is constant $\theta = \theta_b$. Variation of the temperature of the lower substrate enables us to account for the effect of thermal wave propagation along the substrate similar to what was done in previous work [25,26].

In what follows we concentrate on two specific settings, namely, (a) the case of a thin flat lower substrate with a thermal wave propagating along it and (b) the case in which the lower substrate is a thick, periodically corrugated wall with a fixed, spatially uniform temperature on its underside. The spatial coordinates are x and z, where the x axis is placed along the average location of the liquid-solid boundary and the z axis is normal to the latter and directed into the gas phase. The configurations (a) and (b) considered here are shown in Figs. 1(a) and 1(b), respectively.

The material properties of the two fluid components of the system are density ρ_j, dynamic viscosity μ_j, kinematic viscosity ν_j, thermal conductivity k_j, and thermal diffusivity κ_j, where $j = l$ or $j = g$ with subscripts l and g standing for liquid and gas, respectively. Relevant for setting (b), the thermal conductivity of the solid substrate is k_s.

The average thickness of the liquid, gas, and solid [relevant in setting (b)] layers are d, d_g, and d, respectively. The local instantaneous position of the liquid-gas interface is denoted by $h(x,t)$, with t being time, and the geometry of the solid-liquid interface is represented by a periodic function $l(x)$ [$l(x) \equiv 0$ in case (a)], slowly varying with x with the wavelength λ, such that $d \ll \lambda$.

As mentioned above, we also assume that the upper substrate of the system exhibits hydrophobic interaction with the given liquid when they are in a close proximity, so that there exists an energy barrier for a contact between these two phases, and the preferred state of the system is the one where the gas phase always separates the liquid and the solid. In this setting, an actual rupture of the liquid film at the upper substrate does not take place, however it may do so at the lower one. We denote the potential of this hydrophobic interaction by $\tilde{\Pi}_d$.

The film parameter $\epsilon = \frac{d}{\lambda}$ is defined to be the ratio between the mean depth of the liquid film to the wavelength λ of the periodic system in case (b) or a typical wavelength of the interfacial disturbance in case (a). It is assumed to be small, $\epsilon \ll 1$, so it serves as a small parameter in asymptotic expansions as in our previous work [29]. The liquid and gas phases used here are water and air. The relevant physical parameters of the system and dimensionless numbers of the problem are given in Tables I and II, respectively.

TABLE I. Material properties of the system considered in this work.

Physical property	Notation	Value at 20 °C
Layer thickness (water)	d	10^{-4} m
Density (water)	ρ_l	998.3 kg m^{-3}
Thermal diffusivity (water)	κ_l	1.387×10^{-7} m^2 s^{-1}
Kinematic viscosity (water)	ν_l	1.004×10^{-6} m^2 s^{-1}
Thermal conductivity (water)	k_l	0.58 W K^{-1} m^{-1}
Thermal conductivity (air)	k_g	0.0265 W K^{-1} m^{-1}
Surface tension (water-air)	σ	7.23×10^{-2} N m^{-1}
Surface-tension derivative (water-air)	σ_T	1.73×10^{-4} N m^{-1} K^{-1}

In general, it is useful to represent the van der Waals interaction between the liquid and solid in the form of a conjoining-disjoining pressure potential [33]

$$\Pi = \frac{\alpha_3}{y^3} - \frac{\alpha_4}{y^4}, \tag{1}$$

where y is the separation distance between the liquid-gas interface and solid, and α_3 and α_4 are positive Hamaker constants, accounting, respectively, for attractive and repulsive components of the interaction. Note that other forms for Π were used by Teletzke *et al.* [34], Mitlin and Petviashvili [35], and Schwartz and Eley [36].

In what follows we retain only a repulsive component and represent the liquid-solid interaction at the upper hydrophobic plate by a repulsive disjoining pressure potential

$$\tilde{\Pi}_d = -\frac{\tilde{A}_H}{(d + d_g - h)^4}, \tag{2}$$

where $\tilde{A}_H > 0$ is the Hamaker constant [note that α_4 in Eq. (1) is replaced here by $\tilde{A}_H$]. We use the normalization and scaling as in Ref. [29] given in Eq. (6) there,

$$\tau = \frac{\kappa_l t}{d^2}, \quad Z = \frac{z}{d}, \quad \xi = \frac{x}{d}, \quad H = \frac{h}{d}, \tag{3}$$

and follow the derivation carried out by Frumkin and Oron [29], extending it to a possible presence of a thermal wave [26] and hydrophobicity of the upper plate in order to obtain a dimensionless nonlinear evolution equation governing the spatiotemporal dynamics of the gas-liquid interface $Z = H(\xi, \tau)$, accounting for the topography of the underlying substrate $L(\xi) = \frac{1}{d} l(\xi d)$ and $f(\xi, \tau) = \tilde{f}(\xi d, \frac{d^2}{\kappa_l}\tau)$,

TABLE II. Dimensionless numbers of the considered system.

Dimensionless number	Notation	Definition
Thickness ratio	δ	d_g/d
Liquid-solid thermal conductivity ratio	K	k_l/k_s
Marangoni number	M	$\sigma_T \Delta\theta d/\mu_l\kappa_l$
Thermal wave amplitude	a	$A\bar{\theta}_b/\Delta\theta$
Biot number	B	$k_g d/k_l d_g$
Two-layer Biot number	F	$(d/d_g - B)/(1 + B)$
Inverse capillary number	S	$\sigma d/\kappa_l\mu_l$
Hamaker number	A_H	$\epsilon\tilde{A}_H/\mu_l\kappa_l d$

representing a scaled shape of the thermal wave imposed on the underside of the substrate

$$\partial_\tau H + \frac{1}{3}\partial_\xi\left\{(H-L)^3\left[S\partial_\xi^3 H - \partial_\xi \Pi_d(H)\right]\right\} + \frac{1}{2}MB\partial_\xi\left[(H-L)^2\partial_\xi\left(\frac{(1+af)[H-L+K(L+1)]}{(1+B)(1+F-HF)-B[L-K(L+1)]} - af\right)\right] = 0, \quad (4)$$

where $H(\xi,\tau) = \frac{1}{d}h(\xi d, \frac{d^2}{\kappa_l}\tau)$ is the dimensionless position of the liquid-gas interface and $\Pi_d(H)$ is the dimensionless potential of hydrophobic interaction between the liquid and the upper substrate. As in Ref. [26], for a study related to setting (a), the function $f(\xi,\tau)$ is chosen as

$$f(\xi,\tau) = \sin(k\xi - \omega\tau), \quad (5)$$

where $k = \frac{2\pi}{\mathcal{L}}$ is the fundamental wave number of the domain, $\mathcal{L} = \lambda/d = 1/\epsilon$ and ω is the frequency of the thermal wave, both dimensionless.

The two components of the second term in the first line of Eq. (4) represent the effects of capillarity and disjoining pressure, respectively, whereas the terms in its second line account for the effect of thermocapillarity with its combined contributions due to the presence of a thermal wave and the substrate undulation. Equation (4) reduces to Eq. (2.62) in Ref. [14] with disjoining pressure and lower-substrate waviness absent and its uniform temperature, i.e., $\Pi_d = 0$, $a = 0$, and $L(\xi) \equiv 0$. It also reduces to Eq. (3) of Frumkin *et al.* [26] when $\Pi_d = 0$ and $L(\xi) \equiv 0$, and Eq. (19) in Ref. [29] with $\Pi_d = a = 0$.

Expressing the parameter δ via the one- and two-layer Biot numbers B and F, respectively,

$$\delta = \frac{1}{B + F(1+B)},$$

yields the following form of the dimensionless disjoining pressure:

$$\Pi_d(H) = -A_H\left(\frac{B+F(1+B)}{(1+B)(1+F-HF)-BH}\right)^4. \quad (6)$$

Upon substitution of Eq. (6), Eq. (4) is rewritten in its final form as

$$\partial_\tau H + \frac{1}{3}\partial_\xi\left\{(H-L)^3\left[S\partial_\xi^3 H - 4A_H\left(\frac{B+F(1+B)}{(1+B)(1+F-HF)-BH}\right)^5\partial_\xi H\right]\right\} + \frac{1}{2}MB\partial_\xi\left[(H-L)^2\partial_\xi\left(\frac{(1+af)[H-L+K(L+1)]}{(1+B)(1+F-HF)-B[L-K(L+1)]} - af\right)\right] = 0. \quad (7)$$

The local flow rate in the general case is obtained in the form

$$Q_l(\xi,\tau) = \frac{MB}{2}(H-L)^2\partial_\xi\left[\frac{(1+af)[H-L+K(L+1)]}{(1+B)(1+F-HF)-B[L-K(L+1)]} - af\right] + \frac{1}{3}(H-L)^3\left[S\partial_\xi^3 H - 4A_H\left(\frac{B+F(1+B)}{(1+B)(1+F-HF)-BH}\right)^5\partial_\xi H\right]. \quad (8)$$

In the particular case of setting (b), i.e., $a = 0$, the local flow rate is given by

$$Q_l(\xi,\tau) = \frac{MB}{2}(H-L)^2\partial_\xi\left[\frac{H-L+K(L+1)}{(1+B)(1+F-HF)-B[L-K(L+1)]}\right] + \frac{1}{3}(H-L)^3\left[S\partial_\xi^3 H - 4A_H\left(\frac{B+F(1+B)}{(1+B)(1+F-HF)-BH}\right)^5\partial_\xi H\right]. \quad (9)$$

An appropriate scaling for the Hamaker constant yields

$$A_H = \tilde{A}_H \frac{\epsilon}{\mu_l \kappa_l d},$$

where $\tilde{A}_H$ is the dimensional Hamaker constant.

Equation (7) will be used below in our investigation of the system dynamics amended with periodic boundary conditions. In the particular case of a corrugated substrate heated *uniformly* ($a = 0$) from below, at the steady state of the system, if it emerges, the local flow rate $Q_l(\xi,\tau)$ is constant independent of ξ and τ,

$$Q_l = q, \tag{10}$$

and the constant value of q represents the long-time value of the flow rate Q_l averaged over the domain $0 \leqslant \xi \leqslant \mathcal{L} = \frac{\lambda}{d}$,

$$Q = \frac{1}{\mathcal{L}} \int_0^{\mathcal{L}} Q_l d\xi. \tag{11}$$

An explicit expression for the average flow rate through the system subjected to uniform temperature at the underside of the lower substrate can be obtained from the evolution equation (4) by setting $a = 0$. Dividing Eq. (10) combined with Eq. (9) by $(H - L)^2$, integrating the resulting equation over the domain $0 \leqslant \xi \leqslant \mathcal{L}$, using integration by parts with the periodic boundary conditions, and rearranging the term representing the disjoining pressure as

$$\begin{aligned} &4A_H[B + F(1 + B)]^5 \int_0^{\mathcal{L}} \frac{(H - L)\partial_\xi H}{[(1 + B)(1 + F - HF) - BH]^5} d\xi \\ &= A_H[B + F(1 + B)]^4 \int_0^{\mathcal{L}} \frac{\partial_\xi L}{[(1 + B)(1 + F - HF) - BH]^4} d\xi \end{aligned} \tag{12}$$

yields an expression for the average flow rate q in the steady state

$$q = -\frac{\int_0^{\mathcal{L}} \left[SH\partial_\xi^3 L + A_0[(1 + B)(1 + F - HF) - BH]^{-4}\partial_\xi L\right] d\xi}{3\int_0^{\mathcal{L}} (H - L)^{-2} d\xi}, \tag{13}$$

where

$$A_0 = A_H[B + F(1 + B)]^4.$$

Equation (13), apart from standing on its own, will be used to verify numerical results obtained, by comparing the value q provided by Eq. (13) to the direct computation of the long-time average flow rate given by Eqs. (9) and (11) in those cases that result in the emergence of a steady state. We say this from the outset that the comparison is always very favorable.

It is worthwhile to emphasize here that in the regime of traveling wave flow emerging in setting (a) following the transient period, Eq. (13) is also valid in the frame of reference moving with the wave itself, being explicitly independent of a, f, M, and B, since the entire Marangoni term does not explicitly contribute to the value of q vanishing through integration by parts. These parameters affect the shape of the interfacial wave $H(\xi,\tau)$ entering Eq. (13) and therefore affect it implicitly.

In what follows, in the case of a corrugated substrate we set

$$D = 0.3, \quad \delta = 0.5, \quad L(\xi) = D\left[\sin\left(\frac{2\pi\xi}{\mathcal{L}}\right) + 0.25\sin\left(\frac{4\pi\xi}{\mathcal{L}}\right)\right], \tag{14}$$

which was also used in our previous work [29] and serves as a representative example for a left-right asymmetric substrate.

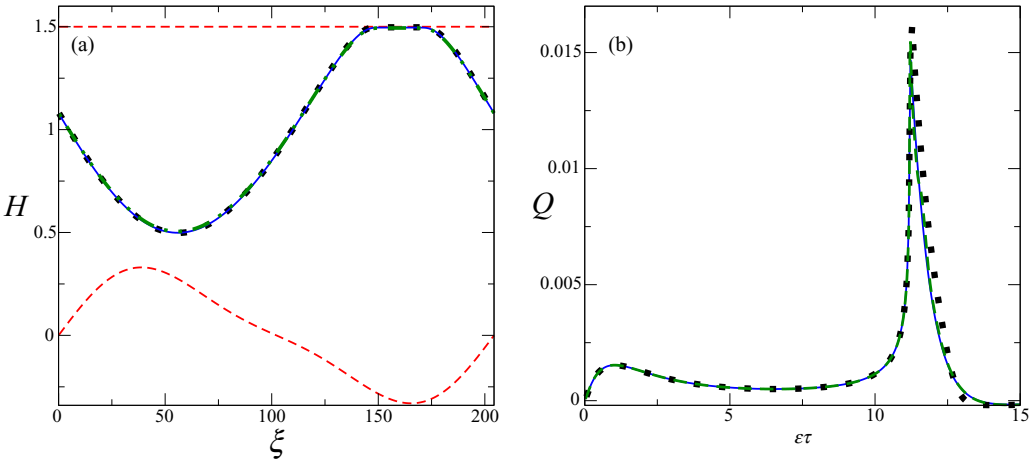

FIG. 2. Comparison showing insensitivity of the system evolution with respect to the choice of the Hamaker constant A_H. The black dots, (green) dashed line, and (blue) solid line correspond to the three different values of A_H determined with the threshold distance of $d + d_g - h \approx 0.1, 0.5, 2.5 \times 10^{-7}$ m, respectively. Here $D = 0.3$ and $K = 0.01$. (a) Liquid-gas interface at $\epsilon\tau = 15$ for these three values of A_H. The dashed curves at the bottom and the top display the lower and upper walls of the system, respectively. Note that at close proximity between the film interface and the upper wall the former flattens out and a thin gap of gas invisible on this scale is formed between the liquid and the wall. (b) Temporal evolution of the average flow rate Q in terms of $\epsilon\tau$ for the three chosen values of A_H.

III. RESULTS AND DISCUSSION

In this section we present the results of our numerical investigation of the system dynamics in the framework of the evolution equation (7) solved along with the initial condition of $H \equiv 1$ and periodic boundary conditions in the domain $0 \leqslant \xi \leqslant \mathcal{L} = \lambda/d \approx 204.313$, as in the previous work [29], using the Newton-Kantorovich method described by Haimovich and Oron [37]. Numerical analysis of the system at hand may pose some serious difficulties due to the disparate scales of the interacting mechanisms. The disjoining pressure term representing van der Waals repulsion becomes significant at distances much smaller than 100 nm (10^{-7} m), thus a reasonable approach would be to turn the disjoining pressure potential on, only for separation distances corresponding to $d + d_g - h < 10^{-7}$ m (or equivalently $1 + \delta - h/d < 10^{-3}$ in the given system), and to set it to be zero otherwise. This approach, however, leads to an abrupt change of the derivatives at $d + d_g - h = 10^{-7}$ m, rendering the numerical computation unstable. Instead, we have found that a continuous form of the potential may be chosen, setting the Hamaker constant to be $\tilde{A}_H = O(10^{-28})$ J, so that the influence of $\Pi_d(H)$ becomes of $O(1)$ at $d + d_g - h \approx 0.5 \times 10^{-7}$ m. We refer to this distance as the threshold distance. This choice for the threshold distance corresponds to $A_H = O(10^{-10})$.

We next check the model sensitivity to the value of the threshold distance and Fig. 2 shows that variation of the value A_H stemming from variation of the threshold distance in a certain range does not have any sizable impact on the resulting dynamics of the system. A further decrease in the value of A_H will not have a significant effect on the system dynamics, but, on the other hand, will greatly increase the temporal resolution required for an adequate performance of numerical computations and thus tremendously increase computational costs.

A. Variation of δ

The previous work [25,26,29] focused on the dynamics of a system with a sufficiently thick gas phase, $\delta \geqslant 3$. As found there in the case of a wavy lower substrate with a constant temperature imposed on its underside, there exists a critical value of the Marangoni number $M = M_c$ so that for

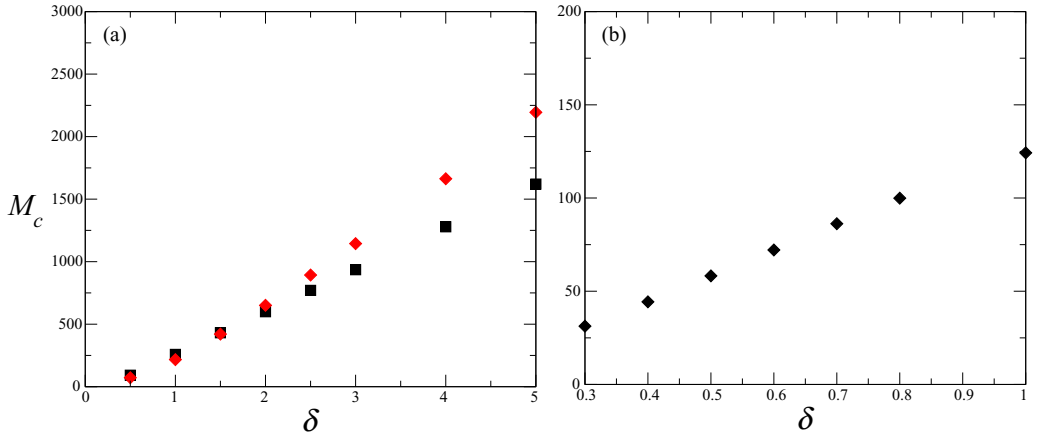

FIG. 3. Variation of the critical Marangoni number M_c with δ. (a) Case (b) with a corrugated lower substrate with $D = 0.3$. Squares and diamonds represent $K = 0.01$ and $K = 1.5$, respectively. (b) Case (a) with a flat lower substrate and its temperature prescribed as a *static* thermal wave with $a = 0.1$.

$M > M_c$ the film ruptures, whereas for $M < M_c$ the film interface reaches a steady deformed state. A qualitatively similar effect takes place when a thermal wave propagates along a flat lower substrate [26], but in this case, the critical value of M depends on ω. These settings allowed the liquid-gas interface to deform and stay away from the upper substrate for $\delta = 3$, preserving the contiguity of the gas layer. In the physical configurations considered in those papers, film rupture took place, when it occurred, on the liquid side.

In a quest for the dynamics in smaller systems, we wish to consider configurations with thinner gas layers, so the value of δ is lower than that used in the earlier work. It is clear that the liquid-solid long-range interaction at the upper surface becomes relevant for sufficiently small values of δ when the deformed film interface approaches it.

If these interactions are neglected, $A_H = 0$, variation of δ affects the critical value of the Marangoni number M_c for both cases of either flat or corrugated lower substrates. A decrease in δ leads to a switching of the location of the film rupture from the lower substrate to the upper one. Since the thickness of the gas layer becomes smaller, the values of M_c become, in the case of a corrugated lower substrate, notably smaller than those presented for $\delta = 3$ [29].

Figure 3(b) presents the dependence of the critical Marangoni number M_c on δ for a flat lower substrate with the temperature profile prescribed as a *static* thermal wave given by Eq. (5) with $\omega = 0$ and the dimensionless amplitude $a = 0.1$. The value of M_c in this case exhibits linear variation with δ and, as expected, the system ruptures for lower values of M as δ decreases. Figure 3(a) depicts the variation of M_c with δ for a corrugated substrate (14) with $D = 0.3$ and the two values of K addressed in Ref. [29], namely, $K = 0.01$ and $K = 1.5$. With a decrease in δ, in both cases, the location of film rupture undergoes a switch from the lower substrate to the upper one. For instance, at $\delta = 2$ rupture takes place at the upper wall for $K = 1.5$ for the first time, whereas for $K = 0.01$ the film still ruptures at the lower substrate. With $\delta \leqslant 1.5$, film rupture takes place at the upper wall for both values of K. Due to the switch of rupture location from the lower substrate to the upper one, the variation of M_c with δ slightly deviates from a linear one. As can be seen in Fig. 3(a), with a decrease in δ, both critical values M_c approach each other and both tend to zero when $\delta \to 0$. It is interesting to note that for $\delta > 1.5$, the critical value of M_c is lower for $K = 0.01$ than for $K = 1.5$. This is explained by the fact that in the former, the trough of the film interface emerges above the crest of the lower substrate, whereas in the latter, this takes place above the substrate depression [29]. This feature results in a locally thinner film in the former than in the latter and in a lower value of the critical Marangoni number M_c since rupture takes place at the lower substrate. In the case

of $\delta \leqslant 1.5$, rupture occurs at the upper wall and the emergence of a hump above the crest of the substrate for $K = 1.5$ rather than above the depression of the substrate when $K = 0.01$ results in a lower value of the critical Marangoni number M_c for $K = 1.5$ than for $K = 0.01$.

B. Flat substrate: Setting (a)

We first consider the case of setting (a), namely, that of a flat substrate on the liquid side of the system. As mentioned in our previous work [26], in the case of a static or slowly moving thermal wave, a competition between the tendency of film rupture either at the liquid-solid boundary or at the gas-solid boundary takes place. If the parameter δ assumes a sufficiently large value, e.g., $\delta = 3$ as in Ref. [26], rupture takes place on the liquid side. However, if δ is sufficiently small, i.e., when the gas layer is sufficiently thin, film rupture occurs on the gas side.

If long-range repulsive interactions at the upper wall are not considered in the case of a traveling thermal wave, film rupture may be prevented when the wave frequency ω is sufficiently large [26] in the case of a relatively thick gas layer. It was also shown there that the amplitude of the interfacial deformation decreases with an increase in ω, hence if the thickness of the gas layer is smaller, a higher frequency is needed to prevent film rupture. However, for small values of δ, these values of ω may go beyond the validity domain of the long-wave approximation.

Inclusion of disjoining pressure in the model allows one to study the system dynamics for smaller values of δ. For a given parameter set of ω, a, and δ, we extend the definition of the critical Marangoni number M_c to $M_c(\omega)$, so for $M > M_c(\omega)$ the film driven by a thermal wave of the frequency ω continues to deform, so the hydrophobic interaction with the upper plate takes place, whereas for $M < M_c(\omega)$, the deformation of the interface remains sufficiently small, so it does not interact with the upper plate. In this sense, the critical value M_c used in the previous work [29] is $M_{c0} \equiv M(\omega = 0)$. The difference, though, will be that due to wider transverse dimensions of the system, film rupture in Ref. [29] took place at the liquid-solid boundary, whereas here, in a narrow configuration, it occurs at the upper plate. We emphasize that the value $M_c(\omega)$ is obtained from numerical solution of Eq. (4).

Figure 4 describes a typical evolution of the liquid-gas interface in terms of the dimensionless time $\epsilon\tau$ for $\delta = 0.5$, $a = 0.1$, and $\omega = 0.002\,447$ for $M = 102.1565$. Note that the corresponding critical Marangoni numbers $M_{c0} \approx 58.23$ and $M_c(\omega) \approx 87.8549$. Here curves 1–8 show the position of the gas-liquid interface at $\epsilon\tau = 0.3, 0.6, 1, 1.5, 2, 2.2, 2.4, 2.8$, respectively. With $M > M_c(\omega)$, the interface deforms until an interaction with the upper plate prevents further deformation and then it flattens out at the tip, as shown by curves 3 and 4. At the same time, the imposed traveling thermal wave forces the interface to travel with it in the longitudinal direction. During this process there is a redistribution of the temperature at the interface with a tendency to reduce temperature gradients, which causes the liquid layer to relax almost back to its nondeformed state, which represents an equilibrium of the system, though unstable in the case of flat substrate. This process then repeats over and over, each time with a more homogeneous temperature distribution at the interface and consequently a smaller interfacial deformation, until it finally settles as a low-amplitude traveling wave away from the bounding walls, as shown in Fig. 5 at $\epsilon\tau = 36$, which represents a traveling state of the system propagating to the right with the velocity of the imposed thermal wave, namely, $v_{\mathrm{TW}} = \frac{\omega}{k}$, with ω and $k = \frac{2\pi}{\mathcal{L}}$ being the dimensionless wave frequency and the fundamental wave number of the thermal wave, respectively.

The time evolution of the difference between the maximal and minimal values of the interfacial temperature variation $\Delta\Theta_s = \Theta_{s,\max} - \Theta_{s,\min}$ is displayed in Fig. 6(a). It first exhibits an oscillatory behavior due to the evolution of the interface intermittently coming into close contact with the upper wall and relaxing due to temperature redistribution leading to a significant decrease in $\Delta\Theta_s$. In the stationary state, $\Delta\Theta_s$ stabilizes at the value of $\Delta\Theta_s \approx 0.2245$ in the case at hand. A qualitatively similar temporal dynamics is observed for the average flow rate Q, as depicted in Fig. 6(b), which converges in the long-time limit to a constant positive value corresponding to the stationary wave flow displayed in Fig. 5.

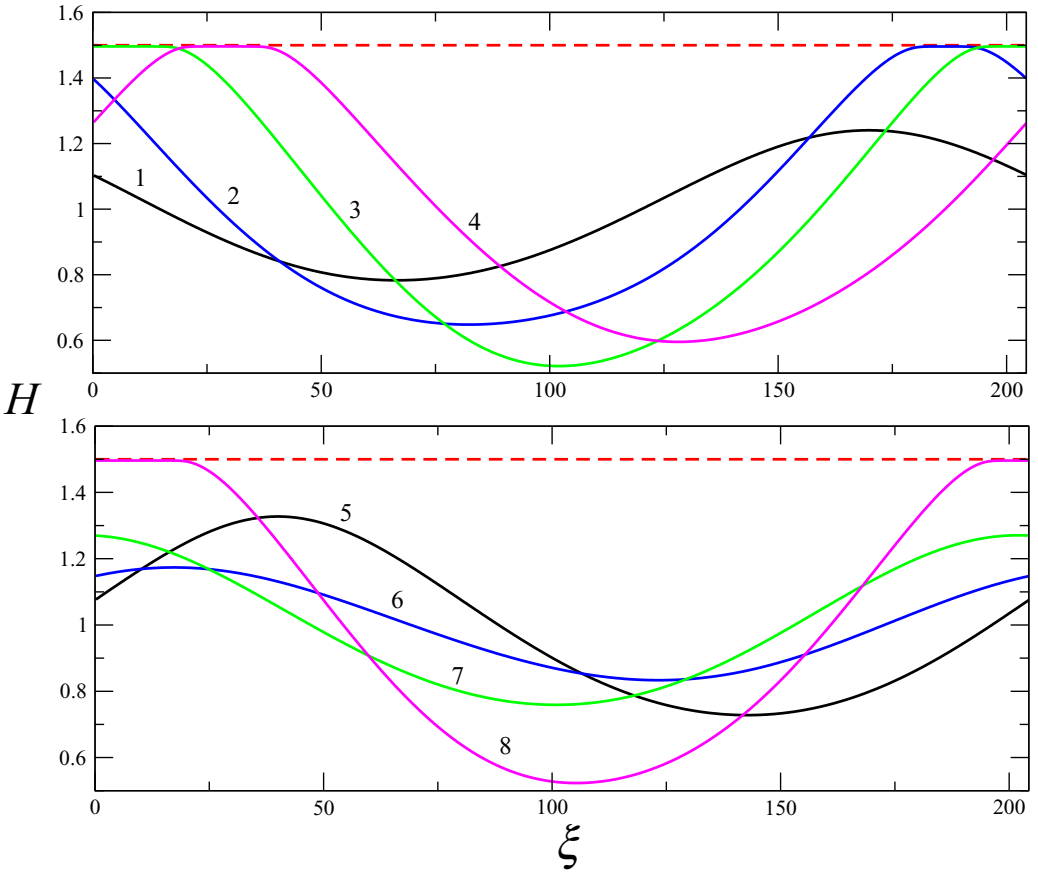

FIG. 4. Spatiotemporal evolution of the gas-liquid interface for $\omega = 0.002\,447$ with $M = 102.15 > M_c(\omega = 0.002\,447)$, $\delta = 0.5$, and $a = 0.1$. Curves 1–8 represent the interfacial shapes at $\epsilon\tau = 0.3, 0.6, 1, 1.5, 2, 2.2, 2.4, 2.8$, respectively. The film interface propagates to the right following the thermal wave. The dashed line represents the upper wall.

Figure 7 depicts the variation of the long-time value of the average flow rate q of the emerging traveling wave flow with the Marangoni number M. It is observed that q increases linearly with M for $M < M_c(\omega)$, whereas for $M > M_c(\omega)$, the increase in q continues more moderately and its variation deviates from linear. We note that the velocity of the traveling wave flow v_{TW} is independent of the Marangoni number M and is prescribed by the value of ω when the wavelength of the thermal wave remains fixed.

Figure 8 depicts the variation with respect to the Marangoni number M of the maximal and minimal values H_{min} and H_{max}, respectively, of the film thickness for traveling wave flows arising in the long-time limit. One of these flows is presented in Fig. 5 for $M = 102.15$. The minimal value H_{min} of the film thickness steadily [and quite linearly, possibly with some change in the slope at $M = M_c \equiv M_c(\omega)$] decreases with M, whereas its maximal value H_{max} increases with M until the critical value $M = M_c(\omega)$ is reached, beyond which H_{max} decreases with M. This behavior can be explained by the following argument: Since the disjoining pressure at the upper wall prevents the film interface from rupture there, as M continues to increase past $M_c(\omega)$, H_{min}, which represents the thickness of the liquid bridges connecting the neighboring droplets formed by the imposed thermal wave, decreases until eventually the liquid film ruptures at the lower substrate. On the other hand, as M increases past $M_c(\omega)$, H_{max} cannot increase beyond the value where the interaction with the

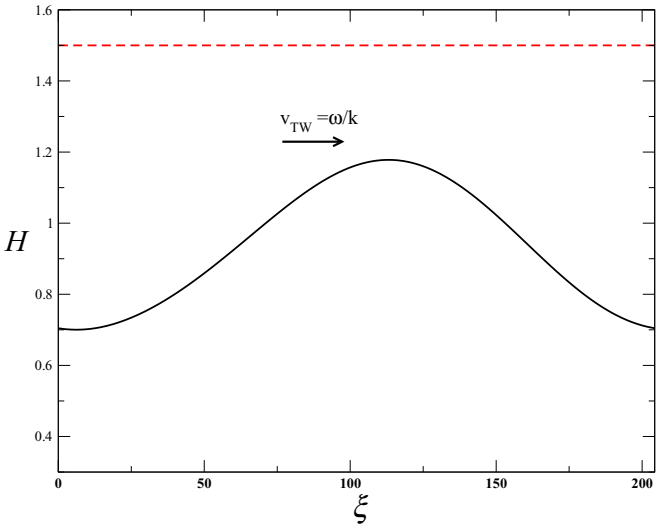

FIG. 5. Traveling wave representing a stationary gas-liquid interface moving to the right with the speed ω/k shown at the dimensionless time $\epsilon\tau = 36$ emerging in the long-time regime of the evolution shown in Fig. 4. Here $\omega = 0.002\,447$ and $k = \frac{2\pi}{\mathcal{L}} \approx 0.03$ is the fundamental wave number. The dashed line represents the upper wall.

upper wall via disjoining pressure begins, which leads to the emergence of flat-top patterns of the liquid-gas interface with a more uniform distribution of the interfacial temperature. As a result, the interfacial humps spread sideways and become less localized and consequently with a lower maximal height $H_{\max}$, with an increase in M for $M > M_c(\omega)$.

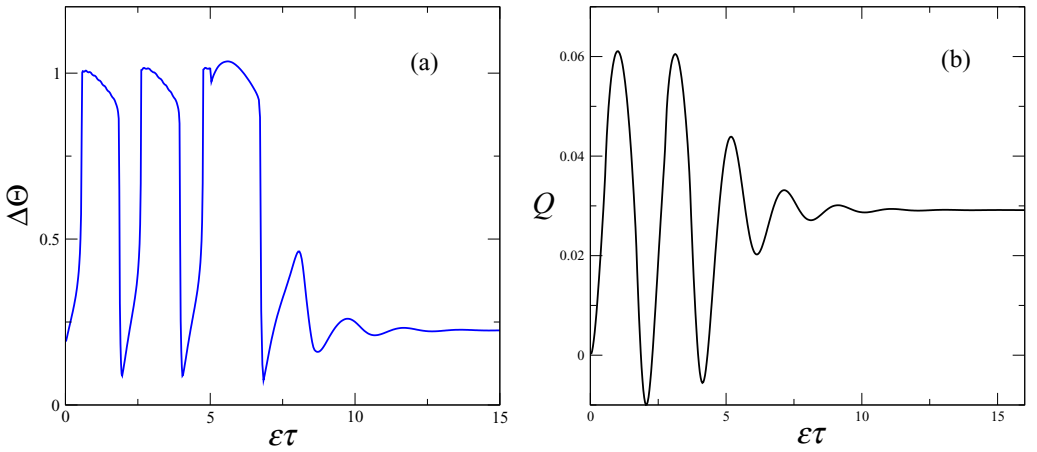

FIG. 6. (a) Temporal variation of the difference $\Delta\Theta_s$ between the maximal and minimal values of the interfacial temperature in terms of the dimensionless time $\epsilon\tau$, for the flow depicted in Figs. 4 and 5. Following an oscillatory transient, the temperature difference settles to a constant value, which is $\Delta\Theta_s \approx 0.2245$ for the given parameter set. (b) Time evolution of the average flow rate in terms of the dimensionless time $\epsilon\tau$ corresponding to the evolution presented in Figs. 4 and 5.

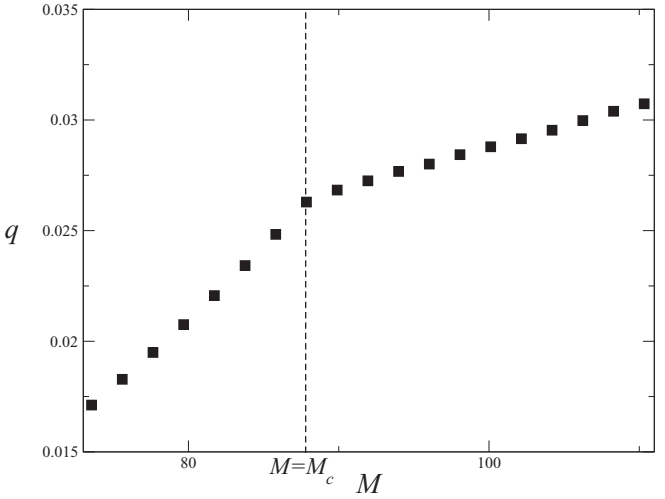

FIG. 7. Variation of the long-time limit of the average flow rate q through the system in its traveling wave regime with the Marangoni number M. Here $a = 0.1$, $\delta = 0.5$, and $\omega = 0.002\,447$.

C. Corrugated substrate: Setting (b)

We now investigate the case (b) of the corrugated lower substrate whose underside is uniformly heated from below, i.e., $a = 0$. The evolution equation (4) now takes the form

$$\partial_\tau H + \frac{1}{3}\partial_\xi\left\{(H-L)^3\left[S\partial_\xi^3 H - \partial_\xi \Pi_d(H)\right]\right\} + \frac{1}{2}MB\partial_\xi\left[(H-L)^2\partial_\xi\left(\frac{H-L+K(L+1)}{(1+B)(1+F-HF)-B[L-K(L+1)]}\right)\right] = 0. \quad (15)$$

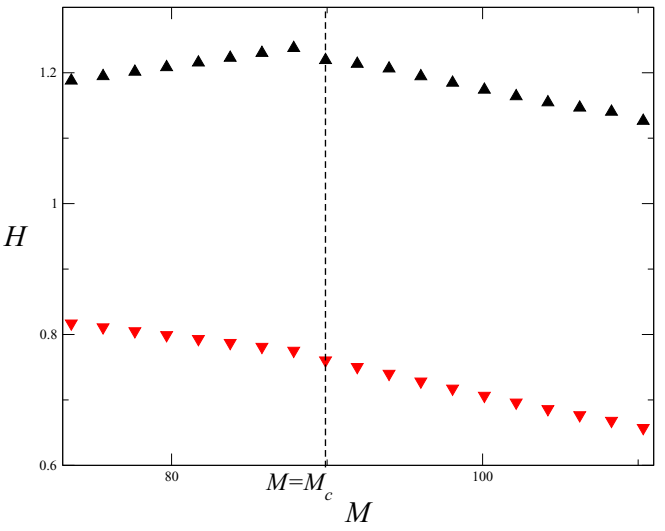

FIG. 8. Variation of the minimal (triangles down) and maximal values (triangles up) of the film thickness in the long-time limit of the evolution in the emerging traveling wave flow. Here $a = 0.1$, $\delta = 0.5$, and $\omega = 0.002\,447$.

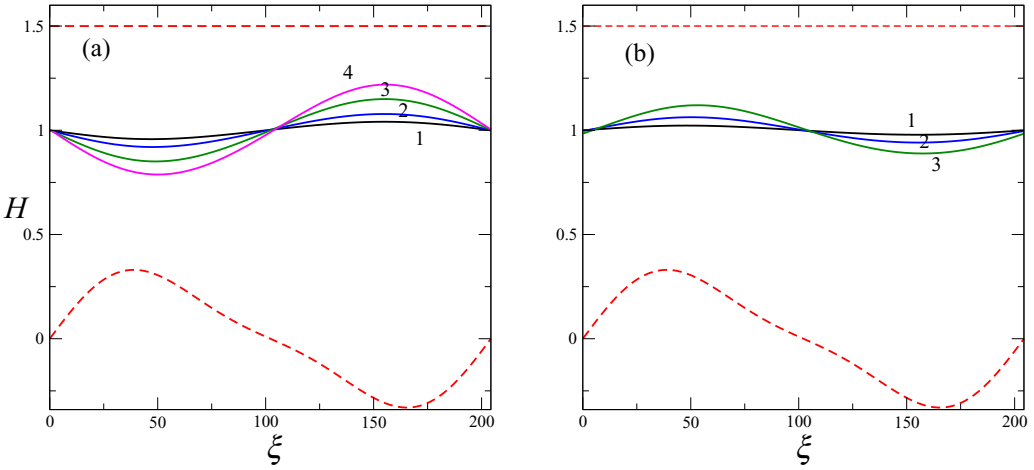

FIG. 9. Steady states of the gas-liquid interface for various values of the Marangoni number for $M < M_{c0}$, $D = 0.3$, and $\delta = 0.5$. The dashed curves represent the upper and lower substrates. (a) $K = 0.01$. Curves 1–4 indicate $M = 40.86$, 61.3, 81.7, and 89.9, respectively. In this case, $M_{c0} = 91.63$. (b) $K = 1.5$. Curves 1–3 indicate $M = 40.86$, 61.3, and 69.46, respectively. In this case, $M_{c0} = 71.59$.

We distinguish between two domains of the Marangoni number M separated by a critical value M_{c0} according to the following rule: For $M < M_{c0}$, the initially flat film interface, which does not represent an equilibrium of the system for $L \neq 0$ with $M \neq 0$, deforms into a steady deformed state of a sufficiently small amplitude; for $M > M_{c0}$, the film interface deforms and finally begins to strongly interact with the hydrophobic upper plate at $Z = 1 + \delta$.

As said above, we concentrate on the parameter set given by Eq. (14). For this parameter set, $M_{c0} \approx 91.63$ for $K = 0.01$ and $M_{c0} \approx 71.59$ for $K = 1.5$, which translate to the temperature differences of $\Delta\theta \approx 0.74$ K and $\Delta\theta \approx 0.57$ K, respectively. Figure 9 presents the gas-liquid interface at its steady state for various values of the Marangoni number $M < M_{c0}$ for $K = 0.01$ [Fig. 9(a)] and $K = 1.5$ [Fig. 9(b)]. As in the case of a thicker gas layer [29] with $\delta = 3$, these steady states of the film interface display humps above the depressions and crests of the lower substrate for $K = 0.01$ and 1.5, respectively. Note that the case of $K = 0.01$ is typical for the situation in which thermal conductivity of the liquid is much lower than that of the substrate as if the latter is made of metal. In contrast, the case of $K = 1.5$ is characteristic of the opposite when the substrate is made of polymer [29] such as poly(dimethyl)siloxane (PDMS).

The temporal evolution of the average flow rate of the respective flows in terms of scaled time $\epsilon\tau$ is displayed in Fig. 10(a) for $K = 0.01$ and in Fig. 10(b) for $K = 1.5$. In the case of $K = 0.01$, the evolution of the average flow rate starts with a positive spike corresponding to the initial deformation of the liquid-gas interface, transforming later into a negative value of the average flow rate. Note that, in our notation, a negative flow rate corresponds to a flow to the left, whereas a positive flow rate represents a flow to the right, i.e., in the direction of the positive $\hat{x}$ axis. In the case of $K = 1.5$, the time evolution of the average flow rate begins with a small negative spike corresponding to the response to the initial deformation of the interface, transforming at a later stage into a positive steady-state value. Note also that the long-time values of the average flow rate q are several orders of magnitude larger for $K = 1.5$ than those for $K = 0.01$.

In the case of $M > M_{c0}$, the film interface continues to deform until it reaches the vicinity of the upper hydrophobic boundary, which is at $Z = 1 + \delta = 1.5$. As mentioned previously, with $K = 0.01$ the highest temperature on the substrate is at its crest, thus the interface deforms in such a way that its trough is positioned above the crest of the substrate. As the interface approaches the upper wall at $Z = 1.5$, it is subjected to the action of the disjoining pressure and a balance between the latter and

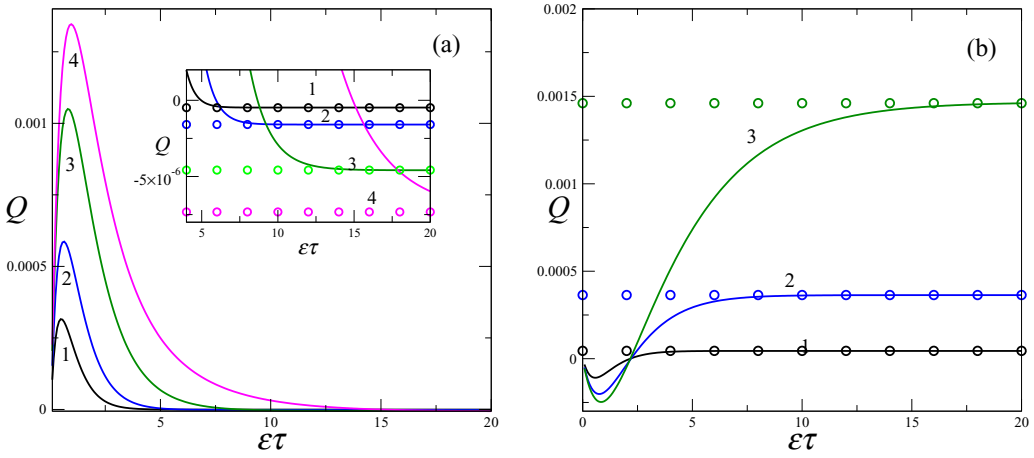

FIG. 10. Temporal evolution of the average flow rate Q in terms of the scaled time $\epsilon\tau$ in the cases leading to the steady states of the film interface for various values of the Marangoni number for $M < M_{c0} = 91.63$, $D = 0.3$, and $\delta = 0.5$. (a) The parameter set is the same as for the cases shown in Fig. 9(a). The inset shows the domain of small negative values of Q. Circles represent the values of q obtained from Eq. (13) and are in a very good agreement with the long-time limit shown by curves 1–4. (b) The parameter set is the same as for the cases shown in Fig. 9(b). Note that the values of Q are shown along the frame on the right.

the thermocapillary drive causes the crest of the interface to deform into a flat-top shape until the system attains its steady state. The latter is shown by curve 3 of Fig. 11(a), displaying the temporal evolution of the liquid-gas interface for $M = 94 > M_{c0} = 91.63$ with $K = 0.01$. Figure 11(b) depicts the corresponding average flow rate Q as a function of the scaled dimensionless time $\epsilon\tau$. The sharp spike in the average flow rate taking place around $\epsilon\tau \approx 12$ corresponds to the abrupt change in the flow as the liquid-gas interface begins its interaction with the hydrophobic wall. The inset in Fig. 11 depicts the average flow rate to the left at the steady state.

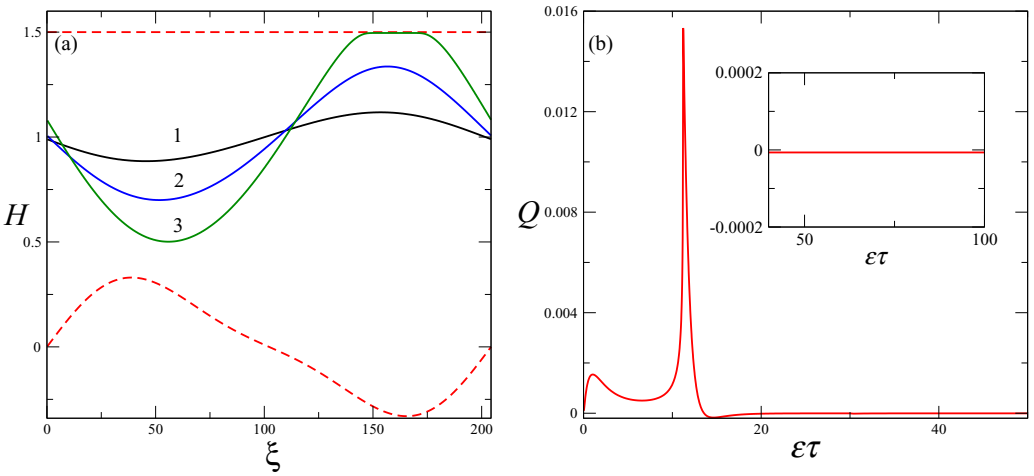

FIG. 11. (a) Temporal evolution of the gas-liquid interface for $M = 94 > M_{c0} = 91.63$, $D = 0.3$, $\delta = 0.5$, and $K = 0.01$. Curves 1–3 correspond to $\epsilon\tau = 1, 10, 15$, respectively, with the latter representing the steady state. The dashed curves represent the upper and lower substrates. (b) Temporal evolution of the average flow rate in terms of scaled dimensionless time $\epsilon\tau$.

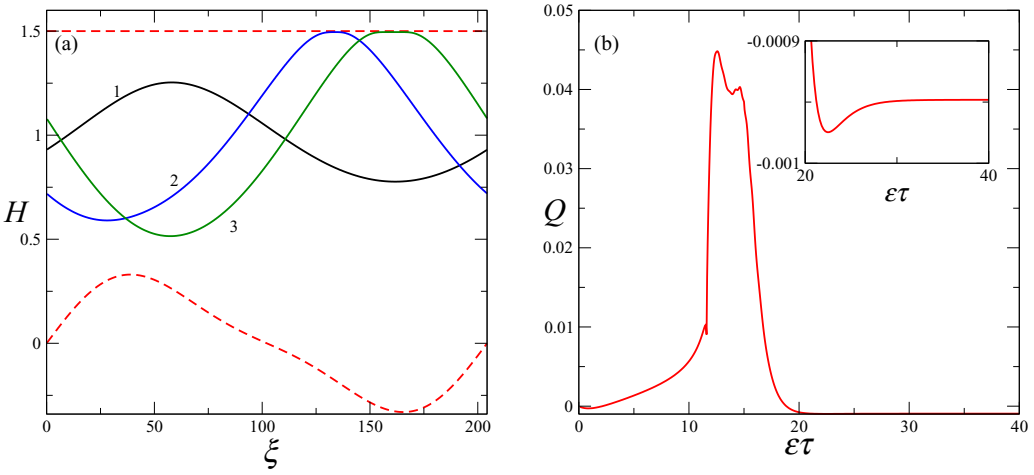

FIG. 12. Film evolution with $M = 73.55 > M_{c0} = 71.59$, $\delta = 0.5$, $D = 0.3$, and $K = 1.5$. (a) Temporal evolution of the gas-liquid interface. Curves 1–3 correspond $\epsilon\tau = 10$, 15, and 20, respectively. The dashed curves represent the upper and lower substrates. Curve 3 corresponds to the steady state of the liquid-gas interface. (b) Variation of the average flow rate Q with the dimensionless time $\epsilon\tau$. The inset shows the large-time variation of Q.

Figure 12(a) presents the evolution of the gas-liquid interface for $K = 1.5$ with curves 1–3 corresponding to $\epsilon\tau = 10$, 15, and 20, respectively, with the latter representing the steady state of the liquid-gas interface. Note that, as compared to the case for $K = 0.01$, here the interface comes to near contact with the upper wall closer to the crest of the lower substrate, after which it slides to the right into a steady-state configuration, where the trough of the interface is positioned approximately above the crest of the lower substrate. The variation of the average flow rate Q with the dimensionless time $\epsilon\tau$ is presented in Fig. 12(b). Apparent sharp changes in the average flow rate are due to displaying the results in the time scale $\epsilon\tau$ and are smooth when shown versus τ. Note also that, as in our previous work [29], the average flow rate at the steady state for $K = 1.5$ is two to three orders of magnitude greater than that for $K = 0.01$.

Figure 13 describes the dependence of the long-time average flow rate q at a steady state of the Marangoni number M for $D = 0.3$, with $K = 0.01$ [Fig. 13(a)] and $K = 1.5$ [Fig. 13(b)]. This figure shows that in both cases $K = 0.01$ and $K = 1.5$, the steady-state value of the average flow rate q increases in its absolute value with an increase in M for $M < M_{c0}$, as indicated by circles, and decreases in its absolute value with an increase in M for $M > M_{c0}$, as marked by squares. At the critical value $M = M_{c0}$, the average flow q is the strongest, i.e., maximal in its absolute value. Note that for $K = 0.01$ the steady flow is directed to the left. However, for $K = 1.5$ the direction of the flow at the steady state changes at $M = M_{c0}$ so that the steady flow is directed to the right for $M < M_{c0}$ and to the left for $M > M_{c0}$.

In the case of $K = 1.5$, the highest temperature on the lower substrate is at its trough, thus the interface deforms in such a way that its crest is positioned above the crest of the substrate, making the film thickness $H - L$ more uniform along the domain. As the crest of the interface approaches $Z = 1.5$, the disjoining pressure at the upper plate hinders a further deformation of the interface in the vertical direction, while the interfacial flow induced by surface-tension gradients pushes the liquid into an equilibrium state, which is where the troughs of the interface are positioned approximately above the crests of the substrate, similar to the case for $K = 0.01$. The effect of film propagation along the system is similar to what was described in our recent paper [29] as a sliding effect.

The emergence of the abrupt change in the direction of the average flow rate in the case of $K = 1.5$ at $M = M_{c0}$ depicted in Fig. 13 is a result of the interface sliding during the interaction

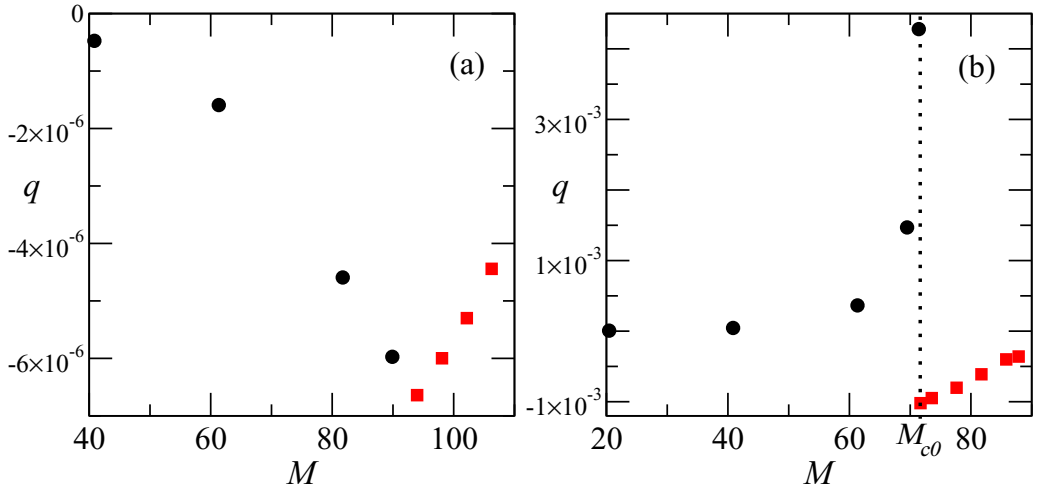

FIG. 13. Variation of the average flow rate q at the long-time steady state with the Marangoni number M for $D = 0.3$ and $\delta = 0.5$. Circles and squares represent values of M below and above the critical Marangoni number M_{c0}, respectively. (a) $K = 0.01$ and $M_{c0} = 91.63$. The average flow rate increases in its absolute value with an increase in M for $M < M_{c0}$ and decreases with an increase in M for $M > M_{c0}$. At $M = M_{c0}$, the average flow is the strongest, i.e., maximal in its absolute value. (b) $K = 1.5$ and $M_{c0} = 71.59$. An abrupt change in the direction of the average flow with the transition of M through M_{c0} takes place.

with the hydrophobic wall in the case of $K = 1.5$, resulting in a final configuration of the interface at a steady state that is qualitatively similar to that achieved for $K = 0.01$. Since the value of the average flow rate is dictated solely by the shape of the liquid-gas interface at a steady state, the resulting values for the average flow rate q are similar in sign for both $K = 0.01$ and $K = 1.5$.

As mentioned above, Fig. 13(b) displays a sharp change in the direction of the average flow rate q at the steady state with the transition of the Marangoni number through $M = M_{c0}$. A careful study of this phenomenon around M_{c0} reveals that there exists a narrow transition region, approximately $M_{c0} - M \leqslant O(10^{-1})$, where the system does not reach a steady state and instead resides in a time-periodic transition state. At this so-called transition state, the Marangoni effect drives the system toward an increase in the amplitude of the interfacial deflection, which leads to an increase in local curvature, which in turn increases the local strength of the stabilizing surface tension, driving the free surface back to a lower-curvature state. This behavior where the initial dominance of the destabilizing Marangoni effect over the stabilizing capillarity changes into the alternating dominance of the latter over the former and back, as the interface deforms, leads to an oscillatory dynamics of the interface, which results in the oscillatory variation of the average flow rate Q as depicted in Fig. 14(a), while the periodicity of the transition state is demonstrated by the phase-plane portrait of the dynamics depicted in Fig. 14(b).

It is important to note that these transition states exist only in the case of $K > 1$, where the asymmetric topography of the substrate induces a horizontal motion of the free surface leading to the inversion of dominance between the Marangoni and the capillary forces. For $0 < K < 1$, the transition through M_{c0} is continuous, as can be seen in Fig. 13(a).

D. Temporal variation of M

In our recent work [29] we demonstrated that temporal variation of the Marangoni number can be used in order to control film dynamics and to significantly increase the average flow rate pumped through the system with the corrugated substrate for $K = 0.01$. Such temporal variation can be achieved through the temporal variation of the temperature difference between the two substrates in

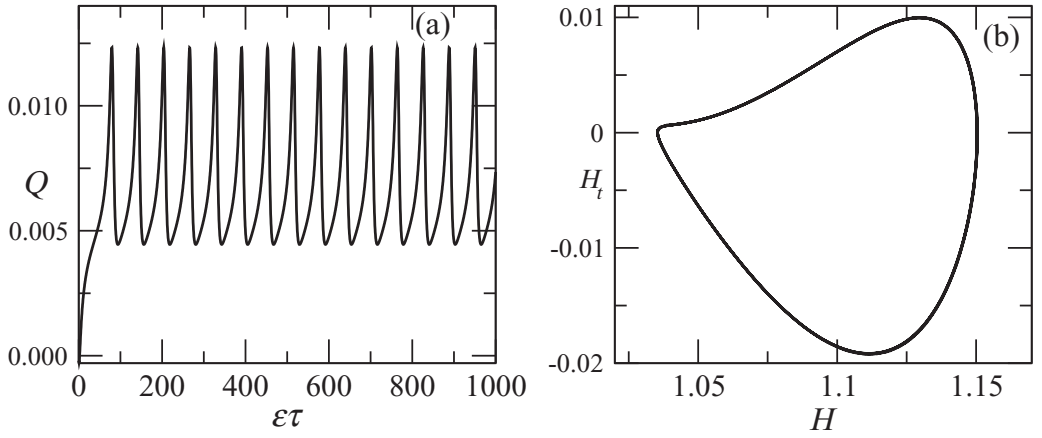

FIG. 14. Dynamics of the system in the transition region for $M = 71.5 < M_{c0} \approx 71.59$ and $K = 1.5$. (a) Average flow rate Q at the transition state as a function of the dimensionless time $\epsilon\tau$. (b) Phase-plane portrait of the dynamics depicted for approximately 15 cycles.

the time scale τ so that the expression af in Eq. (7) represents a function of τ only appropriately prescribed. There we were able to use temporal variation of M to prevent film rupture and to sustain a nonrupturing flow. In this section we apply a similar method to the current setting (b) with hydrophobic interaction for the case with $K = 1.5$ and show that temporally periodic variation of the Marangoni number may lead to the emergence of an almost-time-periodic nonrupturing flow.

The procedure of the imposed temporal variation of M is now delineated as depicted in Fig. 15(a) As shown in Fig. 12, as the crest of the film interface approaches the upper substrate at $Z = 1.5$, it begins to move in the direction where a steady state can be attained, which is, in our case, to the right, until the trough of the interface settles above the crest of the substrate. Once the steady state is approached, we then start to decrease the Marangoni number linearly in time, as shown in Fig. 15(a), to zero until the interface flattens out to $H \equiv 1$ at $M = 0$. Then the Marangoni number is quickly raised back to its initial value of $M = 73.55$ and the process is repeated periodically in time.

Figure 15(b) provides a comparison between the temporal evolution of the average flow rate Q with respect to the dimensionless time $\epsilon\tau$, in the case of the constant $M = 73.55 > M_c$, as shown by the dashed curve, and the temporally varying M for $D = 0.3$ and $K = 1.5$, as presented by the solid curve. The steady-state value of the average flow rate q for the constant value of $M = 73.55$ for this configuration is $q = -0.000\,94$, whereas the value of the average flow rate averaged over one temporal period of forcing is significantly greater $Q_{\text{avg}} = 0.0213$, with the maximal value reaching $Q_{\max} \approx 0.045$, which represents more than a 100-fold enhancement of the flow rate. A nearly periodic character of the emerging flow is observed in Fig. 16, which displays the phase-plane portrait obtained for $H(\xi = 0, \tau)$ for 12 forcing cycles of the flow presented in Fig. 15, where the big square at about $(1.5, -0.2)$ represents a Poincaré section that drifts away slowly, expressing thereby a nearly periodic response of the system. Note that $H_{\epsilon\tau}$ denotes a derivative of H with respect to time $\epsilon\tau$. The spatiotemporal evolution of the liquid-gas interface for approximately one periodic cycle is depicted in Fig. 17. Curves 1–3 describe the evolution of the gas-liquid interface as it tends to settle into a steady state, whereas curves 4–6 describe the relaxation on the interface as it passes through a flat state at $M = 0$ with the decrease in M (curves 4 and 5) and reinitiation of the deformation process with an increase in M (curve 6).

IV. THREE-DIMENSIONAL EXTENSION: SETTING (b)

In this section we study the stability of the steady states in our system with respect to three-dimensional perturbations. We begin by introducing a third spatial dimension $\hat{y}$, to the system under

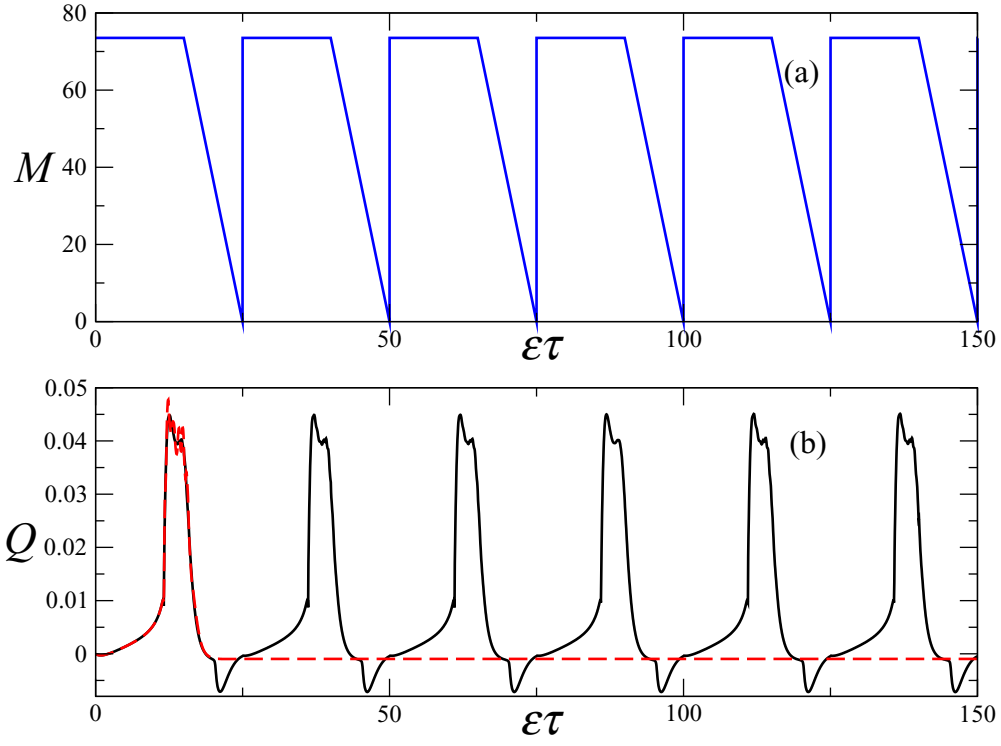

FIG. 15. (a) Temporal variation of the Marangoni number starting with $M = 73.55 > M_{c0} = 71.59$ as in Fig. 12. (b) Temporal variation of the average flow rate Q with the dimensionless time $\epsilon\tau$ for $D = 0.3$ and $K = 1.5$. The dashed curve represents the flow rate for a constant value of $M = 73.55$ decaying to a small negative value as shown in Fig. 12, whereas the solid curve corresponds to the time-dependent Marangoni number shown in (a).

consideration, with the appropriate dimensionless variable $\zeta = \frac{\hat{y}}{d}$. It is assumed that the underlying substrate topography remains two dimensional and is given by Eq. (14).

The three-dimensional evolution equation extending Eq. (7) takes the form

$$\partial_\tau H + \frac{1}{3}\vec{\nabla}\cdot\left[(H-L)^3\left(S\vec{\nabla}\nabla^2 H + 4A_H\left(\frac{B+F(1+B)}{(1+B)(1+F-HF)-BH}\right)^5\vec{\nabla}H\right)\right]$$
$$+\frac{1}{2}MB\vec{\nabla}\cdot\left[(H-L)^2\vec{\nabla}\left(\frac{[H-L+K(L+1)]}{(1+B)(1+F-HF)-B[L-K(L+1)]}\right)\right] = 0, \qquad (16)$$

where $\vec{\nabla} = (\partial_\xi, \partial_\zeta)$. Equation (16) is linearized around the two-dimensional steady state $H_0(\xi)$ as obtained from Eq. (7) by introducing $H(\xi,\zeta,\tau) = H_0(\xi) + \varepsilon\eta(\xi,\zeta,\tau)$, $\varepsilon \ll 1$, where η is a disturbance of the interface at its steady state, which is substituted into the evolution equation (16). Preserving only the $O(\varepsilon)$ terms yields the following equation for the perturbation η:

$$\partial_\tau\eta + \frac{1}{3}S\vec{\nabla}\cdot[3(H_0-L)^2(\vec{\nabla}\nabla^2 H_0)\eta + (H_0-L)^3\vec{\nabla}\nabla^2\eta]$$
$$+4A_H\vec{\nabla}\cdot\left\{(H_0-L)^2\left(\frac{B+F(1+B)}{(1+B)(1+F-HF)-BH}\right)^5\right.$$

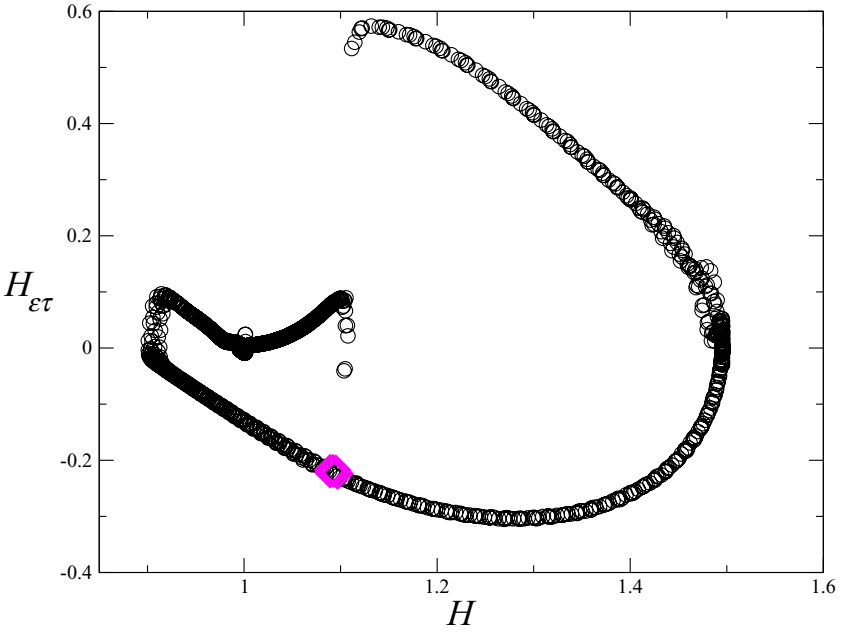

FIG. 16. Phase-plane portrait of $H(\xi = 0,\tau)$ for the case depicted in Fig. 15 with a time-varying M for about 12 cycles. The big square represents a Poincaré section sampled stroboscopically once in a period of forcing, for the duration of eight periods. The Poincaré section at around $(1.5,-0.2)$ is seen to drift slowly away, which shows an almost periodic character of the flow. The apparent jump in $H_{\epsilon\tau}$ around $H \approx 1.12$ is due to the sharp transition in the value of M from 0 to 73.55.

$$\times\left[3\eta\vec{\nabla}H_0+(H_0-L)\vec{\nabla}\eta\left(\frac{5(B+F(1+B))}{(1+B)(1+F-HF)-BH}+1\right)\right]\Bigg\}$$
$$+MB\vec{\nabla}\cdot\left[(H_0-L)\eta\vec{\nabla}\left(\frac{H_0-L+K(L+1)}{(1+B)(1+F-H_0F)-B[L-K(L+1)]}\right)\right]$$
$$+\frac{1}{2}MB\vec{\nabla}\cdot\left[(H_0-L)^2\vec{\nabla}\left(\frac{\eta}{(1+B)(1+F-H_0F)-B[L-K(L+1)]}\right.\right.$$
$$\left.\left.+\frac{F(1+B)(H_0-\tilde{L}+K)\eta}{\{(1+B)(1+F-H_0F)-B[L-K(L+1)]\}^2}\right)\right]=0. \tag{17}$$

Substituting a normal form $H_1 = J(\xi)e^{ik_y\zeta+\lambda_y\tau}$ into Eq. (17) yields the periodic eigenvalue problem for the function $J(\xi)$,

$$-\lambda_y J=\alpha_y(H_0)J_{\xi\xi\xi\xi}+\beta_y(H_0)J_{\xi\xi\xi}+\gamma_y(H_0;k_y)J_{\xi\xi}+\delta_y(H_0)J_\xi+\epsilon_y(H_0;k_y)J, \tag{18}$$

from which the growth rate λ_y of the perturbation can be evaluated. The coefficients $\alpha_y,\beta_y,\gamma_y,\delta_y,\epsilon_y$ are given in the Appendix.

We proceed by numerically solving Eq. (18) in terms of function $J(\xi)$ and the eigenvalues λ_y with periodic boundary conditions in $0 \leqslant \xi \leqslant \mathcal{L}$ for different values of the wave number k_y, starting from $k_y = 0$. The numerical solution is obtained via the MATLAB Chebfun package [38], which uses a spectral expansion in Chebyshev polynomials and solves sets of linear homogeneous ordinary differential equations and eigenvalue problems with general boundary conditions.

As in Sec. III, we study two qualitatively different domains of the parameter K, namely, $K < 1$ and $K > 1$. In addition, we distinguish between two domains of the Marangoni number, namely,

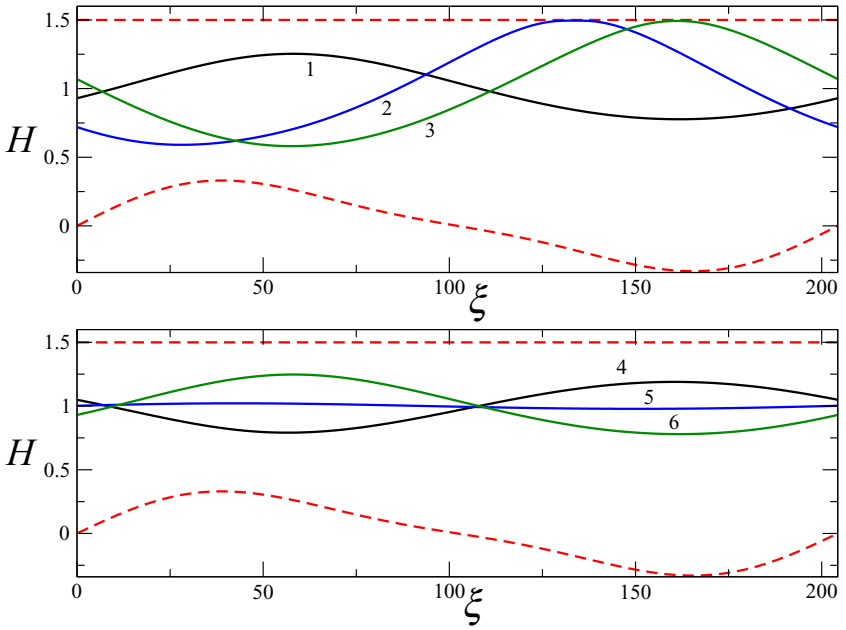

FIG. 17. Spatiotemporal evolution of the liquid-gas interface for approximately one forcing period. Curves 1–6 represent the film interface at $\epsilon\tau = 10$, 15, 20, 22, 25, and 35, respectively, with $D = 0.3$ and $K = 1.5$. The dashed curves represent the upper and lower substrates.

$M < M_{c0}$, where the steady state is reached without interaction with the hydrophobic plate, and $M > M_{c0}$, where the interface at the steady state is in contact with the upper plate.

We define ρ_y as the maximal real part of the eigenvalues

$$\rho_y = \max[\mathrm{Re}(\lambda_y; k_y)], \tag{19}$$

with Re denoting the real part of the corresponding variable; thus spatial perturbations with $\rho_y < 0$ will decay in time, while those with $\rho_y > 0$ will amplify in time τ. For steady states attained by the gas-liquid interface with $M < M_{c0}$, i.e., when the hydrophobic interaction between the film interface and the upper wall can be neglected, we find that in both cases ($K < 1$ and $K > 1$) for sufficiently low values of the Marangoni number M, the value ρ_y is always negative, thus the corresponding two-dimensional steady state is stable to perturbations for any values of the wave number k_y. When the Marangoni number M exceeds a certain threshold, ρ_y is positive for values of k_y smaller than a value of the transition threshold k_y^0 depending on the Marangoni number, making the base two-dimensional steady state unstable to perturbations with a sufficiently long wavelength in the $\hat{y}$ direction. Perturbations with $k_y > k_y^0$ have $\rho_y < 0$ and the corresponding two-dimensional steady state is thus stable for disturbances with a shorter wavelength. Figure 18 depicts the variation of the value ρ_y with k_y for several values of the Marangoni number in the range of $M < M_{c0}$, with $\delta = 0.5$ and $D = 0.3$. The growth rate ρ_y of the disturbance is found to monotonically decrease with its wave number k_y for a fixed Marangoni number and to increase with the Marangoni number for a fixed k_y.

For values of M slightly above M_{c0}, the liquid-gas interface deforms until it comes into close contact with the hydrophobic upper plate. In this case, we find that ρ_y is always negative, thus the corresponding two-dimensional steady states are stable to perturbations with any wave number k_y for both $K < 1$ and $K > 1$. Figure 19 displays the variation of ρ_y with k_y for $K < 1$ and $K > 1$, with $\delta = 0.5$ and $D = 0.3$. Similarly to the previous case shown in Fig. 18, the growth rate ρ_y decreases

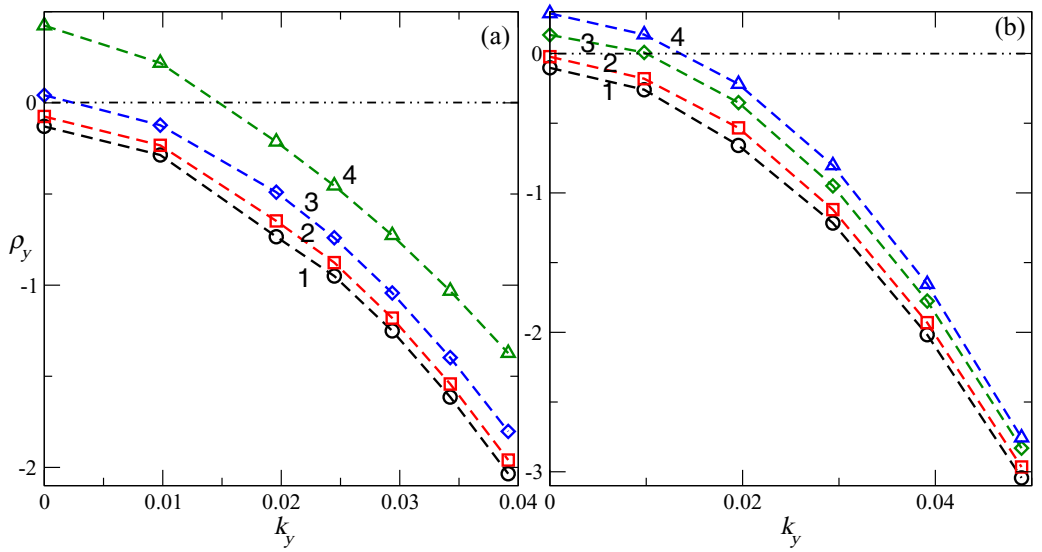

FIG. 18. Variation of ρ_y with the wave number k_y of a transverse disturbance for $\delta = 0.5$ and $D = 0.3$. (a) Curves 1–4 represent different values of the Marangoni number $M = 10.21, 20.43, 40.86, 81.72$, respectively, with $K = 0.01$ and $M_{c0} = 91.63$. (b) Curves 1–4 represent different values of the Marangoni number $M = 10.21, 20.43, 40.86, 61.3$, respectively, with $K = 1.5$ and $M_{c0} = 71.59$. In both cases, for M below a certain threshold, the value $\rho_y < 0$ for any k_y demonstrating stability of the corresponding steady flows with respect to transverse disturbances.

with k_y for a fixed Marangoni number for a larger K. In contradistinction to the previous case, the case of a low K displays a nonmonotonic variation of ρ_y with k_y.

These results can be given the following physical interpretation. In the case of $M < M_{c0}$, the mechanism of stabilization and destabilization is similar to that of a flat film resting on a flat surface, since both the film interface in the base state and the topography of the solid substrate in the transverse direction are flat. Thus, for lower values of M and shorter domains the interface

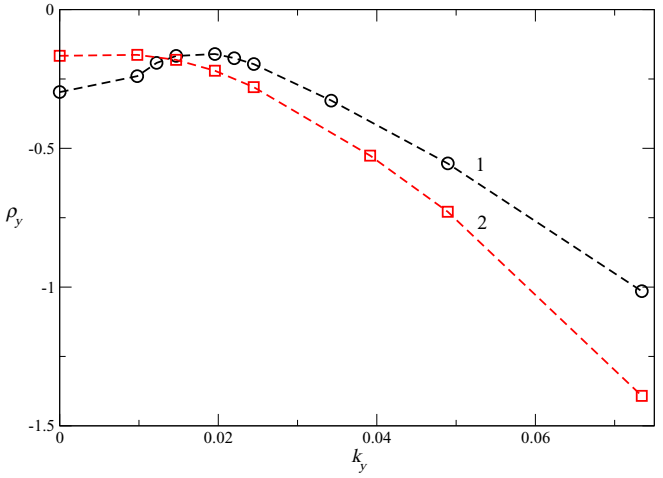

FIG. 19. Variation of ρ_y with the wave number k_y for $M > M_{c0}$. Curves 1 and 2 represent the cases of $K = 0.01$ and $M = 102.15 > M_{c0}$, and $K = 1.5$ and $M = 73.6 > M_{c0}$, respectively.

that is flat in the transverse direction will remain stable to infinitesimal perturbations in the same direction, while an increase in M or in the periodicity-domain size will lead to destabilization of the flat configuration through long-wave disturbances. For $M > M_{c0}$, the two-dimensional gas-liquid interface settles into a deflected steady state with a flat-top segment whose separation distance from the cooled upper substrate is determined by the hydrophobic repulsion. This deflected configuration of the interface is maintained by a strong interfacial flow from the lower warmer regions to the colder upper ones. An infinitesimal perturbation of a zero total volume in the transverse direction will tend to deform the gas-liquid interface in both the longitudinal and the transverse directions, being restrained by the inability of the interface to reduce the separation distance from the upper substrate due to hydrophobic repulsion. As a result of this, the two-dimensional curved steady state will be restored.

In both cases $M > M_{c0}$ and $M < M_{c0}$, the two-dimensional steady states exhibit robustness with respect to infinitesimal disturbances in the third dimension except for long-wave disturbances with the wavelength larger than the wavelength of the substrate corrugation in the latter case. Note that $k_y = 0.02$ representing a typical value for the transition threshold k_y^0 corresponds to the wavelength $\mathcal{L}_y = 100\pi > \mathcal{L} \approx 204.313$ used here. This suggests that the results presented in this work in the context of the two-dimensional configuration may be applicable to real physical systems.

V. SUMMARY

In this paper we have extended our previous analysis [26,29] and investigated the dynamics of a horizontal two-layer two-dimensional gas-liquid system sandwiched between a solid hydrophobic wall from above and a heat conducting substrate from below. The upper wall is assumed to be held at a constant temperature θ_t, while the lower substrate is of a general periodic topography $l(x)$, heated from below to a spatiotemporally varying temperature $\theta_b(x,t)$. Two particular cases were considered: (a) a flat lower substrate of an imposed temperature profile in the form of a traveling thermal wave and (b) the lower substrate of a thick periodically corrugated topography that is uniformly heated on its underside.

We have demonstrated that hydrophobicity of the upper wall enables a continuous flow in narrow systems corresponding to low values of the parameter δ and prevents the liquid-gas interface from rupturing at the upper wall. In setting (a) with a liquid film deposited on a flat underlying substrate with a traveling thermal wave imposed there, if the Marangoni number M or the thermal amplitude A are taken to be sufficiently large, the liquid-gas interface will deform following the propagating thermal wave until close contact is made with the upper wall. Due to the repulsive effect of disjoining pressure, the interface does not rupture at the upper wall but instead rebounds several times, and following each close contact with the upper wall the interface flattens out at its tip, leading to a more uniform distribution of the interfacial temperature. As a result, the system dynamics results in the emergence of a traveling wave flow of a relatively small interfacial deformation following the propagating thermal wave.

In setting (b) with a thin liquid film overlying a corrugated substrate, in the case of the Marangoni number greater than its critical value, the interface deforms toward rupture at the upper wall until its interaction with the latter through the disjoining pressure. The liquid-gas interface finally settles into a steady state, allowing for a nonzero average flow rate through the system. We have found that these *two-dimensional* steady states are linearly stable to small disturbances in the transverse out-of-plane direction for either sufficiently small or sufficiently (but not too) large values of the Marangoni number. In the intermediate range of the Marangoni number, the two-dimensional steady states are linearly unstable to long-wave out-of-plane disturbances and stable to the shorter ones. It is also noteworthy that there exists a range near the critical value of the Marangoni number $M = M_{c0}$ where steady states do not develop, giving way to the emergence of temporally periodic evolution of the system.

We have also revealed that temporally periodic variation of the temperature difference across the system may be harnessed to significantly increase an otherwise small flow rate in a steady

flow, turning the steady flow into an almost periodic one. In contrast with our previous work [29], quite simple temporal modulation of the Marangoni number leads to both an almost-time-periodic evolution of the film and an almost-time-periodic pumping effect of the liquid through the system. It appears that the presence of a hydrophobic wall assists through the recurrence of flat-top patterns in its vicinity to regularize the modulated flow.

Introduction of hydrophobicity of the upper wall allows for a continuous operation of two-layer gas-liquid systems with a very thin gas layer, making the system very responsive to weak differential heating across the system. This mechanism may be employed in a design of small-size transport devices treating biological samples with a strong sensitivity to temperature variations.

ACKNOWLEDGMENT

The research of A.O. was partially supported by Israel Science Foundation Grant No. 345/13 and by David T. Siegel Chair in Fluid Mechanics.

APPENDIX: COEFFICIENTS OF THE EIGENPROBLEM FOR THE THREE-DIMENSIONAL STABILITY ANALYSIS

The coefficients for Eq. (18) are given by the expressions

$$\alpha_y(H_0) = \frac{S}{3}(H_0 - L)^3, \quad \beta_y(H_0) = S(H_{0\xi} - L_\xi)(H_0 - L)^2,$$

$$\begin{aligned}\gamma_y(H_0; k_y) = &-\frac{2S}{3}k_y^2(H_0 - L)^3 + \frac{1}{2}MB(H_0 - L)^2\left[\frac{1}{(1+B)(1+F-H_0F) - B(\bar{L}-K)}\right.\\ &\left.+\frac{F(1+B)(H_0 - \bar{L} + K)}{[(1+B)(1+F-H_0F) - B(\bar{L}-K)]^2}\right]\\ &+4A_H\left[(H_0 - L)^3\left(\frac{B + F(1+B)}{(1+B)(1+F-FH_0) - BH_0}\right)^5\right.\\ &\left.\times\left(\frac{5(B+F(1+B))}{(1+B)(1+F-FH_0) - BH_0} + 1\right)\right],\end{aligned}$$

$$\begin{aligned}\delta_y(H_0) = &S(H_0 - L)^2 H_{0\xi\xi\xi} + MB(H_0 - L)\left(\frac{H_0 - \bar{L} + K}{(1+B)(1+F-H_0F) - B(\bar{L}-K)}\right)_\xi\\ &+\frac{MB}{2}\frac{[(H_0 - L)^2]_\xi}{(1+B)(1+F-H_0F) - B(\bar{L}-K)}\\ &\times\left[1 + \frac{F(1+B)(H_0 - \bar{L} + K)}{(1+B)(1+F-H_0F) - B(\bar{L}-K)}\right]\\ &+4A_H\left\{\left[(H_0 - L)^2\left(\frac{5[B+F(1+B)]}{(1+B)(1+F-FH_0) - BH_0}\right)^5\right]_\xi\right.\\ &\times\left(\frac{5[B+F(1+B)]}{(1+B)(1+F-FH_0) - BH_0} + 1\right)(H_0 - L) + 3H_{0\xi}(H_0 - L)^2\\ &\left.\times\left(\frac{B+F(1+B)}{(1+B)(1+F-FH_0) - BH_0}\right)^5\right\},\end{aligned}$$

$$\epsilon_y(H_0;k_y) = SH_{0\xi\xi\xi\xi}(H_0-L)^2 + 2SH_{0\xi}(H_{0\xi}-L_\xi) + \frac{S}{3}k_y^4(H_0-L)^3$$
$$+ MB\left[(H_0-L)\left(\frac{H_0-\bar{L}+K}{(1+B)(1+F-H_0F)-B(\bar{L}-K)}\right)_\xi\right]_\xi$$
$$+ \frac{1}{2}MB\left[(H_0-L)^2\left(\frac{1}{(1+B)(1+F-H_0F)-B(\bar{L}-K)}\right.\right.$$
$$\left.\left.+ \frac{F(1+B)(H_0-\bar{L}+K)}{[(1+B)(1+F-H_0F)-B(\bar{L}-K)]^2}\right)_\xi\right]_\xi$$
$$- \frac{MB}{2}\frac{(H_0-L)^2k_y^2}{(1+B)(1+F-H_0F)-B(\bar{L}-K)}$$
$$\times\left[1+\frac{F(1+B)(H_0-\bar{L}+K)}{(1+B)(1+F-H_0F)-B(\bar{L}-K)}\right]$$
$$+ 4A_H\left\{\left[(H_0-L)^2\left(\frac{5[B+F(1+B)]}{(1+B)(1+F-FH_0)-BH_0}\right)^5\right]_\xi 3H_{0\xi}\right.$$
$$+ (H_0-L)^2\left(\frac{5[B+F(1+B)]}{(1+B)(1+F-FH_0)-BH_0}\right)^5\left[3H_{0\xi\xi}-k_y^2(H_0-L)\right.$$
$$\left.\left.\times\left(\frac{5[B+F(1+B)]}{(1+B)(1+F-FH_0)-BH_0}+1\right)\right]\right\},$$

where $\bar{L} = (1-K)L$.

[1] D. Figeys and D. Pinto, Lab-on-a-chip: A revolution in biological and medical sciences, Anal. Chem. **72**, 330 A (2000).

[2] H. A. Stone and S. Kim, Microfluidics: Basic issues, applications, and challenges, AIChE J. **47**, 1250 (2001).

[3] C. G. M. Marangoni, Über die ausbreitung der tropfen einer flüssigkeit auf der oberfläche einer anderen, Ann. Phys. Chem. **143**, 337 (1871).

[4] T. S. Sammarco and M. A. Burns, Thermocapillary pumping of discrete drops in microfabricated analysis devices, AIChE J. **45**, 350 (1999).

[5] F. D. D. Santos and T. Ondarcuhu, Free-Running Droplets, Phys. Rev. Lett. **75**, 2972 (1995).

[6] K. Ichimura, S. K. Oh, and M. Nakagawa, Light-driven motion of liquids on a photoresponsive surface, Science **288**, 1624 (2000).

[7] E. Schäffer, T. Thurn-Albrecht, T. P. Russell, and U. Steiner, Electrically induced structure formation and pattern transfer, Nature (London) **403**, 874 (2000).

[8] J. Lee and C.-J. Kim, Surface-tension-driven microactuation based on continuous electrowetting, J. Microelectromech. Syst. **9**, 171 (2000).

[9] J. R. A. Pearson, On convection cells induced by surface tension, J. Fluid Mech. **4**, 489 (1958).

[10] H. Bénard, Les tourbillons cellulaires dans une nappe liquide, Rev. Gen. Sci. Pures Appl. **11**, 1261 (1900).

[11] S. H. Davis, Thermocapillary instabilities, Annu. Rev. Fluid Mech. **19**, 403 (1987).

[12] A. A. Nepomnyashchy, M. G. Velarde, and P. Colinet, *Interfacial Phenomena and Convection* (Chapman and Hall/CRC, Boca Raton, 2002).

[13] A. Karbalaei, R. Kumar, and H.-J. Cho, Thermocapillarity in microfluidics—A review, Micromachines **7**, 13 (2016), and references therein.
[14] A. Oron, S. H. Davis, and S. G. Bankoff, Long-scale evolution of thin liquid films, Rev. Mod. Phys. **69**, 931 (1997).
[15] A. Sheludko, Thin liquid films, Adv. Colloid Interface Sci. **1**, 391 (1967).
[16] A. Oron and P. Rosenau, Formation of patterns induced by thermocapillarity and gravity, J. Phys. (France) II **2**, 131 (1992).
[17] B. K. Kopbosynov and V. V. Pukhnachev, Thermocapillary flow in thin liquid films, Fluid Mech. Sov. Res. **15**, 95 (1986).
[18] A. Oron, Nonlinear dynamics of three-dimensional long-wave Marangoni instability in thin liquid films, Phys. Fluids **12**, 1633 (2000).
[19] A. A. Golovin, A. A. Nepomnyashchy, and L. M. Pismen, Interaction between short-scale Marangoni convection and long-scale deformational instability, Phys. Fluids **6**, 34 (1994).
[20] S. J. VanHook, M. F. Schatz, J. B. Swift, W. D. McCormick, and H. L. Swinney, Long-wavelength surface-tension-driven Bénard convection: Experiment and theory, J. Fluid Mech. **345**, 45 (1997).
[21] R. D. Lenz and S. Kumar, Steady two-layer flow in a topographically patterned channel, Phys. Fluids **19**, 102103 (2007).
[22] S. K. Kalpathy, L. F. Francis, and S. Kumar, Shear-induced suppression of rupture in two-layer thin liquid films, J. Colloid Interface Sci. **348**, 271 (2010).
[23] M. J. Davis, M. B. Gratton, and S. H. Davis, Suppressing van der Waals driven rupture through shear, J. Fluid Mech. **661**, 522 (2010).
[24] A. A. Darhuber and S. M. Troian, Principles of microfluidic actuation by modulation of surface stresses, Annu. Rev. Fluid Mech. **37**, 425 (2005).
[25] W. Mao, A. Oron, and A. Alexeev, Fluid transport in thin liquid films using traveling thermal waves, Phys. Fluids **25**, 072101 (2013).
[26] V. Frumkin, W. Mao, A. Alexeev, and A. Oron, Creating localized-droplet train by traveling thermal waves, Phys. Fluids **26**, 082108 (2014).
[27] A. D. Stroock, R. F. Ismagilov, H. A. Stone, and G. M. Whitesides, Fluidic ratchet based on Marangoni-Benard convection, Langmuir **19**, 4358 (2003).
[28] H. Linke, B. J. Aleman, L. D. Melling, M. J. Taormina, M. J. Francis, C. C. Dow-Hygelund, V. Narayanan, R. P. Taylor, and A. Stout, Self-Propelled Leidenfrost Droplets, Phys. Rev. Lett. **96**, 154502 (2006).
[29] V. Frumkin and A. Oron, Liquid film flow along a substrate with an asymmetric topography sustained by the thermocapillary effect, Phys. Fluids **28**, 082107 (2016).
[30] C. Neto, D. R. Evans, E. Bonaccurso, H. J. Butt, and V. S. J. Craig, Boundary slip in Newtonian liquids: A review of experimental studies, Rep. Prog. Phys. **68**, 2859 (2005).
[31] J. P. Rothstein, Slip on superhydrophobic surfaces, Annu. Rev. Fluid Mech. **42**, 89 (2010).
[32] O. I. Vinogradova, Slippage of water over hydrophobic surfaces, Int. J. Miner. Process. **56**, 31 (1999).
[33] A. Oron and S. G. Bankoff, Dewetting of a heated surface by an evaporating liquid film under conjoining/disjoining pressures, J. Colloid Interface Sci. **218**, 152 (1999).
[34] G. F. Teletzke, H. T. Davis, and L. E. Scriven, Wetting hydrodynamics, Rev. Phys. Appl. **23**, 989 (1988).
[35] V. S. Mitlin and N. V. Petviashvili, Nonlinear dynamics of dewetting: Kinetically stable structures, Phys. Lett. A **192**, 323 (1994).
[36] L. W. Schwartz and R. R. Eley, Simulation of droplet motion on low-energy and heterogeneous surfaces, J. Colloid Interface Sci. **202**, 173 (1998).
[37] O. Haimovich and A. Oron, Nonlinear dynamics of a thin liquid film on an axially oscillating cylindrical surface, Phys. Fluids **22**, 032101 (2010).
[38] MATLAB Chebfun package: http://www.chebfun.org.